High-Resolution Imaging with Adaptive Optics in Patients with Inherited Retinal Degeneration

Jacque L. Duncan,[1] *Yuhua Zhang,*[2] *Jarel Gandhi,*[1] *Chiaki Nakanishi,*[1] *Mohammad Othman,*[3] *Kari E. H. Branham,*[3] *Anand Swaroop,*[3,4] *and Austin Roorda*[2]

Purpose. To investigate macular photoreceptor structure in patients with inherited retinal degeneration using high-resolution images and to correlate the findings with clinical phenotypes and genetic mutations.

Methods. Adaptive optics scanning laser ophthalmoscopy (AOSLO) images of photoreceptors were obtained in 16 eyes: five with retinitis pigmentosa (RP), three with cone-rod dystrophy (CRD), and eight without retinal disease. A quadratic model was used to illustrate cone spacing as a function of retinal eccentricity. Cone spacing at 1° eccentricity was compared with standard measures of central visual function, including best-corrected visual acuity (BCVA), foveal threshold, and multifocal electroretinogram (mfERG) amplitude and timing. Intervisit variations were studied in one patient with RP and one patient with CRD. Screening of candidate disease genes identified mutations in two patients, one with RP (a rhodopsin mutation) and the other with CRD (a novel *RPGR*-ORF15 mutation).

Results. Cone spacing values were significantly different from normal for patients with RP ($P = 0.01$) and CRD ($P < 0.0001$) and demonstrated a statistically significant correlation with foveal threshold ($P = 0.0003$), BCVA ($P = 0.01$), and mfERG amplitude ($P = 0.008$). Although many RP patients showed normal cone spacing within 1° of fixation, cones could not be unambiguously identified in several retinal regions. Cone spacing increased in all CRD patients, even those with early disease. Little variation was observed in cone spacing measured during two sessions fewer than 8 days apart.

Conclusions. AOSLO images can be used to study macular cones with high resolution in patients with retinal degeneration. The authors present the first report of cone structure in vivo in patients with mutations in rhodopsin and *RPGR*-ORF15 and show that macular cones display distinct characteristics, depending on the underlying disease. AOSLO imaging, therefore, can provide new insight into possible mechanisms of cone vision loss in patients with retinal degeneration. (*Invest Ophthalmol Vis Sci.* 2007;48:3283–3291) DOI:10.1167/iovs.06-1422

Retinal degenerations constitute a group of inherited diseases that result in progressive death of photoreceptors. In retinitis pigmentosa (RP), cone dysfunction is secondary to rod degeneration and ultimately results in loss of fine visual acuity.[1] The mechanism of cone death in patients with RP, often caused by rod-specific mutations, remains unclear,[2–4] in part because photoreceptors cannot be easily visualized in living eyes. The blur caused by irregularities of the eye's optics limits the resolution of retinal images with the methods commonly used in clinical practice.[5] Adaptive optics (AO) can compensate for these aberrations and has been used to provide high-resolution retinal images.[6–13] Scanning laser ophthalmoscopy (SLO) provides the ability to record images in real time, to obtain high-contrast retinal images, and to optically section the tissue.[14] The integration of AO into SLO—AOSLO—further improves the resolution and contrast resulting from the superior rejection of light from out-of-focus layers.[15–17] After correcting aberrations, lateral resolutions on the order of 2 μm can be achieved, thereby allowing visualization of single-cone photoreceptors.[18,19] Recent studies have demonstrated the feasibility of using AO to image cones in the maculas of patients with retinal degeneration, including those with cone-rod dystrophy (CRD).[20,21] However, all but one patient studied to date has undergone imaging using flood-illuminated AO systems.[20,21]

The present study was designed to evaluate, with the use of a clinically deployable AOSLO system, a larger number of patients with retinal degeneration and unaffected controls than had been reported previously.[20,21] To better understand the relationship between rod and cone survival in patients with RP and CRD, we obtained high-resolution cone images from such patients. We then correlated measures of cone spacing with common clinical measures of macular cone structure and function in patients with these two types of retinal dystrophy, as reported earlier.[20,21] However, in contrast to previous studies, we used an AOSLO with an infrared light source, thereby minimizing exposure to visible light, which is reported to increase disease severity in animal models of retinal degeneration[22–26]; we identified genetic mutations in two patients and investigated these with the use of AOSLO; we correlated high-resolution macular cone images with high-resolution fundus–guided perimetry results; and we obtained images of patients twice within 8 days to determine the reproducibility of AOSLO cone measures.

Subjects and Methods

Research procedures were performed in accordance with the Declaration of Helsinki. The study protocol was approved by the institu-

From the [1]Department of Ophthalmology, University of California, San Francisco School of Medicine, San Francisco, California; [2]School of Optometry, University of California at Berkeley, Berkeley, California; and the Departments of [3]Ophthalmology and Visual Sciences and [4]Human Genetics, University of Michigan, Ann Arbor, Michigan.

Supported by a Career Development Award from Research to Prevent Blindness; the Foundation Fighting Blindness (JLD, AS); National Eye Institute Grants EY00415 (JLD), EY14375 (AR), and EY007961 (AS); That Man May See, Inc.; The Bernard A. Newcomb Macular Degeneration Fund (JLD); and the Elmer and Sylvia Sramek Foundation (AS); and the National Science Foundation Science and Technology Center for Adaptive Optics, managed by the University of California at Santa Cruz under cooperative agreement AST-9876783.

Submitted for publication December 1, 2006; revised February 2 and 22, 2007; accepted April 16, 2007.

Disclosure: **J.L. Duncan**, None; **Y. Zhang**, None; **J. Gandhi**, None; **C. Nakanishi**, None; **M. Othman**, None; **K.E.H. Branham**, None; **A. Swaroop**, None; **A. Roorda**, Optos PLC (C), University of Houston, University of Rochester (P)

The publication costs of this article were defrayed in part by page charge payment. This article must therefore be marked "*advertisement*" in accordance with 18 U.S.C. §1734 solely to indicate this fact.

Corresponding author: Jacque L. Duncan, Department of Ophthalmology, Room K-129, University of California, San Francisco School of Medicine, 10 Koret Way, San Francisco, CA 94143-0730; duncanj@vision.ucsf.edu.

tional review boards of the University of California, San Francisco, the University of California at Berkeley, and the University of Michigan. All subjects gave written informed consent before participation in the studies.

Clinical Examination

The study population consisted of 16 eyes, from five patients with RP, three patients with CRD, and eight subjects with unaffected eyes (Table 1). Each patient and each subject with healthy eyes underwent complete eye examination. All patients and three subjects with healthy eyes (subject ages 20, 27, and 61 years) underwent additional clinical testing that included testing of color vision, visual field, multifocal electroretinography (ERG), optical coherence tomography (OCT), and measurement of best-corrected visual acuity (BCVA) with a Snellen chart and reported as the quotient of the Snellen acuity (20/20 = 1.0). Acuities equal to or better than 20/20 were recorded as 20/20. Patients were excluded if their pupils did not dilate to at least 7 mm, they had dense cataracts or other media opacities, they had previously undergone refractive surgery, they had pseudophakia, or they were unable to maintain stable fixation on a 1° target. Color vision was assessed with the use of a color vision test (Farnsworth D-15 panel; Richmond Products, Inc., Albuquerque, NM). Subjects showing no crossing errors on the color vision test were further examined with a Lanthony 15-hue desaturated panel. Automated perimetry was completed with a visual field analyzer (Humphrey Visual Field Analyzer II; 750-6116-12.6; Carl Zeiss Meditec, Inc., Dublin, CA), 10-2 Swedish interactive thresholding algorithm (SITA) with measurement of foveal thresholds, a Goldmann III stimulus on a white background (31.5 ASB), and an exposure duration of 200 ms. Goldmann kinetic perimetry was performed with V-4e and I-4e targets. Fundus-related microperimetry was examined in a subset of subjects (MP-1; Nidek Technologies America Inc., Greensboro, NC). The central 8° visual field was tested with a Goldmann III stimulus of 200-ms duration with a 4-2 threshold strategy; subjects were instructed to fixate on the center of four crosses, each 2° in size at an eccentricity of 5°. Fixation was monitored with respect to the fovea—judged by anatomic landmarks—and stability. Numeric thresholds in decibels (dB) were exported and overlain with AOSLO images (Matlab software; Mathworks, Natick, MA). OCT images were obtained (Stratus OCT 4.0.2 software; Zeiss Instruments, Dublin, CA) to determine retinal thickness with 6-mm horizontal scans centered on the anatomic fovea. Retinal thickness was measured using calipers to mark the vitread surface of the foveal dip and the first highly reflective band sclerad to the vitread surface. Pupils were dilated with 1% tropicamide and 2.5% phenylephrine before full-field ERG, which was performed after 45 minutes of dark adaptation using a Burian-Allen contact lens electrode (Hansen Ophthalmic Development Laboratory, Iowa City, IA), according to International Society for Clinical Electrophysiology and Vision (ISCEV)[27] standards. Multifocal ERG (mfERG) testing was performed in a light-adapted state (VERIS 5.1.10×; Electro-Diagnostic Imaging, Inc., Redwood City, CA) with a Burian-Allen contact lens

Table 1. Clinical Characteristics of the Patients Studied

Patient/ Symbol	Age (y)	Sex	Diagnosis/ Genotype	VA	Foveal Threshold (dB)	Color Testing/ Axis	Goldmann Visual Field	Full-Field ERG	mfERG Amplitude (μV)	mfERG Timing (msec)
RP 1/X	26	F	Simplex RP	1.0	36	Normal	20° central island	Mixed scotopic reduced 70% and delayed, photopic reduced 80% and delayed	48.2	25.8
RP 2/open circles	33	M	Simplex RP	1.0	37	Normal	Absolute scotoma 30°–60° inferior to fixation	Mixed scotopic reduced 70% and delayed, photopic reduced 50% and delayed	77.1	27.5
RP 3/open squares	33	F	ADRP/rhodopsin Gly51Val	1.0	37	NT	Absolute ring scotoma 10°–60° from fixation	Mixed scotopic reduced 20% and delayed, photopic normal	55.4	28.3
RP 4/open diamonds	37	F	Simplex RP	0.5	31	7/Tritan	Absolute ring scotoma 20°–50° from fixation	Mixed scotopic NR, photopic severely reduced	16.4	24.2
RP 5/open triangles	43	F	Simplex RP	1.0	34	Normal	Absolute scotoma 10°–30° superior to fixation	Mixed scotopic NR, photopic severely reduced	35.3	30.8
CRD 1/filled diamonds	32	M	XLCRD/*RPGR* ORF15 Glu481 GlyfsX492	1.0	27	3/Tritan	Full to V4e and I4e	Scotopic normal, photopic reduced 40% below normal	20.1	30.8
CRD 2/filled triangles	41	M	Simplex CRD	0.4	23	8/Mixed	Absolute 5° diameter central scotoma	Scotopic normal, photopic reduced 20% below normal	14.2	35.8
CRD 3/filled circles	42	M	Simplex CRD	0.3	26	6/Mixed	Full to V4e and I4e	Scotopic normal, photopic reduced 20% below normal	24.9	36.7

Symbols refer to those in Figures 4 and 7. RP, retinitis pigmentosa; CRD, cone rod dystrophy; AD, autosomal dominant; XL, X-linked; VA, visual acuity in the study eye; color testing, number of crossing errors using a Farnsworth D-15 panel; axis, axis of confusion; normal, no crossing errors; NT, not tested; NR, not recordable; mfERG, multifocal electroretinogram P1 response measured from the central trace. Full-field ERG responses are reported for dark-adapted mixed rod and cone b-waves (scotopic) and light-adapted single flash b-waves (photopic); values are given as percentage below the lower limits of normal for our laboratory. Genotype is reported only for patients in whom molecular analysis revealed disease-causing mutations in genes, as described in Methods.

electrode according to ISCEV standards.[28] Responses were recorded using 16 30-second sequences in each eye. The stimulus consisted of 103 elements covering the central 40° diameter of the visual field; the flash intensity was 200 cd/m^2, the intensity of dark frames was less than 4 cd/m^2, and the average luminance was 100 cd/m^2. Fixation was monitored with the use of an infrared eye camera. The signal was amplified 100,000 times, and the bandwidth measured 10 to 100 Hz. A single iteration of 17% spatial averaging was performed (VERIS software; Electro-Diagnostic Imaging, Inc.). Response amplitudes of the first-order waveform were measured from N1-P1, and P1 response latency was reported.

Mutation Screening

One patient with X-linked (XL) CRD was screened, on a research basis, for mutations in the *RPGR* gene previously associated with cone-rod dystrophies.[29–33] Molecular analysis of rhodopsin, *RDS*, and *RP1* was performed on patients with autosomal dominant (AD) RP, and analysis of the *CRX* and *ABCA4* genes was performed on patients with CRD. These tests were chosen because genetic testing was available on a fee-for-service basis, performed by CLIA-certified laboratories (University of Iowa Diagnostic Laboratories and Carver Laboratory for Molecular Diagnosis, Iowa City, IA; and University of Michigan Ophthalmic Molecular Diagnostic Laboratory, Ann Arbor, MI).

AOSLO Image Acquisition

All patients and eight subjects with healthy eyes (subjects' ages 20, 26, 27, 27, 39, 40, 57, and 61) underwent AOSLO. The eye with better visual acuity or more stable fixation was chosen for imaging studies. A dental impression mount was used to stabilize head position. Briefly, the AOSLO system makes use of a low-coherence, 840-nm light source, a Shack-Hartman wavefront sensor, and a 140-actuator microelectromachined (MEMS) deformable mirror (Boston Micromachines Corporation, Watertown, MA).[18] Digital videos were recorded at 25 locations surrounding fixation, extending 2° from fixation, and obtained at 0.5° intervals. Additional videos were recorded in regions of relative or absolute scotoma in each patient and in comparable regions in a subset of subjects with healthy eyes.

AOSLO Image Analysis

Distortions in images caused by eye movements were eliminated with the use of customized software.[34,35] After correction, static frames were averaged to enhance the signal-to-noise ratio. These images were then organized (Adobe Photoshop; Adobe Systems Inc., Mountain View, CA) by aligning landmarks on overlapping images to create a continuous 4° montage of macular cones surrounding fixation.

Cone Spacing Analysis

Image scales were computed from calibration images of a model eye, recorded before each imaging session. Regions of the image in which a contiguous cone mosaic was clearly visible were selected, and the power spectrum was computed using ImageJ software (version 1.3 6b with Java 1.5.0_06; http://rsb.info.nih.gov/ij; National Institutes of Health, Bethesda, MD). The location of each analyzed region was determined with respect to the fovea from the montage image. Spatial frequency of the ring in the power spectrum, corresponding to the cone-sampling frequency,[36] was manually identified at up to eight locations on the ring and was then converted to angular cone spacing using the following equation, assuming hexagonal packing of the cone mosaic: center-to-center spacing = line spacing/cos (π/6).

Whenever a ring in the power spectrum was not clearly resolved, individual cones were identified manually. Average nearest-neighbor spacing was determined from the first peak in the density recovery profile (DRP), a method devised by Rodieck[37] to quantify the spatial arrangement of cells.[9] DRP plots the average histogram of density of all cells surrounding each cell in the mosaic as a function of distance from the central cone. Figure 1 describes both analysis methods. Cone spacing was chosen as a metric because it provided the most robust and conservative measurement for comparison among eyes. Alternative methods, such as cone-packing density, are unreliable unless all cones in a region can be confidently identified, whereas fast Fourier transform (FFT)–based methods and cone spacing estimated from manual selection do not require all cones in the mosaic to be visible.

To confirm our cone spacing measurements, histologic data from the literature[38] were converted from cones/mm^2 to cone spacing in arcminutes on the retina using a conversion factor of 282 μm = 1°.[38] This conversion assumes hexagonal cone packing, which may slightly underestimate cone spacing in retinal locations with amorphous cone packing.

Statistical Analysis

The best model to describe cone spacing measurements as a function of degrees of eccentricity from the fovea was determined (version 9.1; SAS Institute, Cary, NC). Statistical analysis (SAS Proc Mixed; SAS Institute) was used to fit the model to accommodate repeated measurements that were taken on two subjects. Empiric evaluation of the plots of data for each subject suggested that a quadratic model should fit the data well in the range of retinal eccentricity over which cone spacing data were collected. Individual subjects appeared to have different intercepts and slopes, so these terms were entered into the model as random effects. In a preliminary analysis, the intercept, linear coefficient, and quadratic coefficient were entered as random effects. The final model included degree, degree^2, disease status (normal is reference group), interaction of degree and disease status, and the interaction of degree^2 and disease status as fixed effects. The estimated quadratic model was used to generate a curve predicting the mean normal cone spacing with the 95% prediction range (PR) at each eccentricity; curves for RP and CRD patients were generated in a similar manner. RP and CRD curves were then compared with the normal curve using a likelihood ratio test. The test value can be referred to a χ^2 value with 3 df. Because unambiguous cones were not identified within 0.5° of fixation in most subjects, cone spacing for each patient was estimated from the model for each patient at a single location, 1° eccentric to the fovea. These values were then used to correlate with measures of central visual function, including BCVA, automated perimetry thresholds, mfERG amplitudes and timing using a two-tailed Pearson correlation coefficient (GraphPad Prism version 4.0c for Macintosh; GraphPad Software, San Diego, CA). $P < 0.05$ was considered statistically significant.

Results

Cone Spacing Measured by AOSLO in Subjects with Healthy Eyes Compared Favorably with Histologic Data from the Literature

Figure 2A shows an AOSLO image of the photoreceptor mosaic 1° from the fovea of a healthy eye. Every photoreceptor was resolved at this retinal location. A continuous montage of photoreceptor images surrounding the fovea was created in subjects with healthy eyes, providing unambiguous visualization of cone arrays that were readily quantified throughout the central macula. Quantification of cone spacing at a number of retinal eccentricities for eight healthy eyes is shown in Figure 2B. Mean cone spacing ± 1 SD is indicated for each measurement. Values predicted by the quadratic model and 95% PR of normal cone spacing measured using AOSLO compared favorably with the mean ± 2 SD of cone spacing that was measured histologically,[38] despite different measurement techniques and the use of live human subjects.

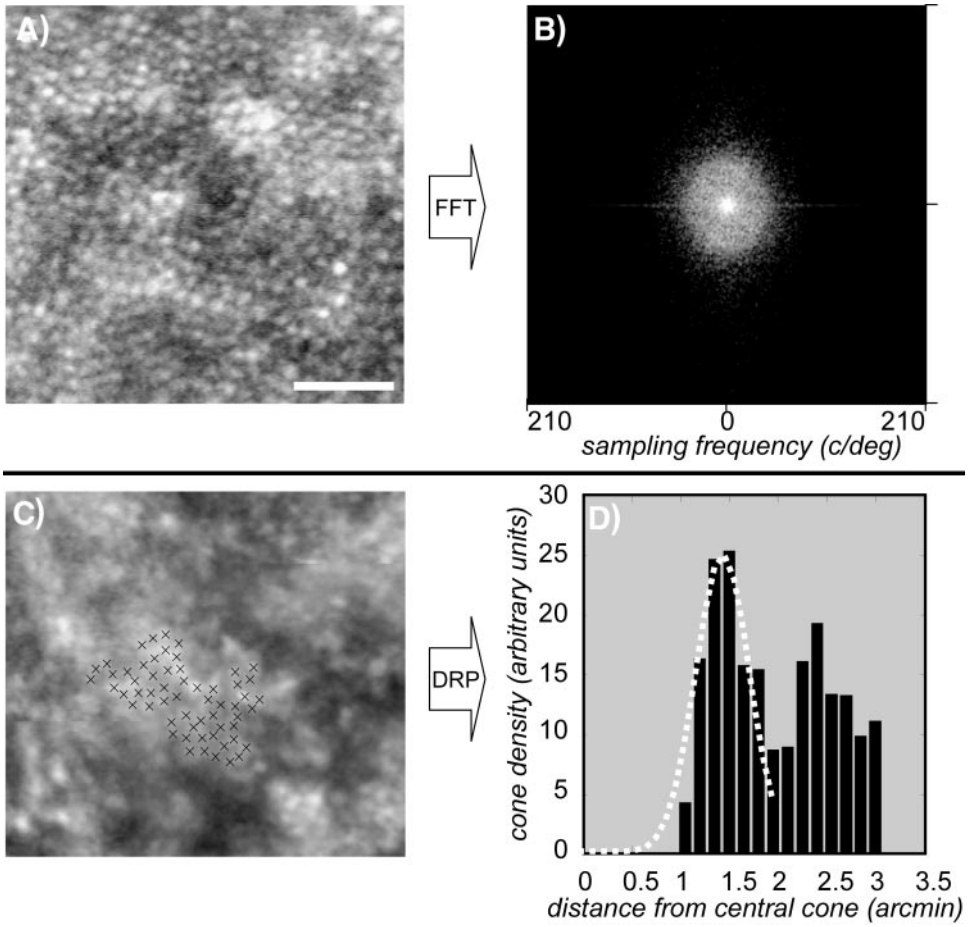

FIGURE 1. (**A**, **B**) FFT for measuring cone spacing. (**A**) Cropped section of the image from patient CRD 1. Not every cone is resolved. (**B**) Power spectrum of the cone image. The ring indicates the sampling density of the cone mosaic. The slight hexagonal appearance of the ring indicates that the cones are hexagonally packed at this location. (**C**, **D**) DRP for measuring cone spacing. (**C**) Cropped section of the image from patient RP 4. Each mark indicates a manually labeled cone. (**D**) Average cone density in expanding annular rings about each selected cone. The first peak indicates the nearest-neighbor distance, or average cone spacing. Gaussian fit to the first peak in the DRP is used to compute the average nearest-neighbor cone spacing.

Cones Were Readily Imaged with the Use of AOSLO in Patients with Retinal Degeneration

High-resolution macular cone images were obtained in all eight patients with retinal degenerative diseases, including one patient (RP 1) with a small central posterior subcapsular cataract and cystoid macular edema (CME). Clinical characteristics of the patients are summarized in Table 1. Fixation was stable and located within 0.5° of the anatomic fovea in all patients, as determined by minimal retinal thickness on OCT and fixation testing during microperimetry. None of the patients demonstrated fundus flecks or a dark choroid, and the patient with XL CRD revealed no tapetal-like sheen.[39] Genetic mutations were identified in two patients. One patient with autosomal dominant retinitis pigmentosa (ADRP) (RP 3) showed a heterozygous GGC>GTC nucleotide substitution in codon 51 of the rhodopsin gene, resulting in an amino acid change of Gly51Val. Another patient with XL CRD (CRD 1) demonstrated a deletion in exon ORF15 of *RPGR* (ORF+1443_1444 delGA) resulting in a frameshift mutation, Glu481GlyfsX492. This novel mutation is at the 3′ end of ORF15, where other mutations from patients with XL CRD have been reported.[29–33] An example of cone images obtained from each of these patients, RP 1 (top), RP 3 (middle), and CRD 1 (bottom), is shown in Figure 3. A contiguous cone mosaic with normal cone spacing was detected in patient RP 1, whereas patchy regions of cone loss were seen adjacent to regions with more normal cone spacing in patient RP 3, the patient with ADRP carrying a rhodopsin mutation. Patient CRD 1 had a contiguous cone mosaic with increased cone spacing.

A summary of cone spacing for all eight patients examined is shown in Figure 4. Cone spacing was analyzed using the FFT method for all patients except CRD 1, CRD 3, and RP 1, whose images were analyzed according to the DRP method. Although normal macular cone spacing was observed in many patients with RP, when evaluated as a group, cone structures near the foveas of patients with RP were significantly different for subjects with healthy eyes and for CRD patients. Comparison of the curve for patients with RP and subjects with healthy eyes yielded a test statistic of 11.3 ($P = 0.01$). Similarly, comparison of patients with CRD and subjects with healthy eyes yielded a test statistic of 33.5 ($P < 0.0001$). At 1° from the fovea, mean cone spacing was 20% greater than normal for RP patients and 70% greater than normal for CRD patients. In addition to significant quantitative differences in cone spacing, qualitative abnormalities were observed in AOSLO images from patients with retinal degeneration. For example, despite the presence of many locations with quantifiable cones, there were patches in which cones could not be identified reliably throughout the maculas of RP patients. This phenomenon was not observed in healthy eyes. Figure 5 shows AOSLO images within 2° of the fovea of patient RP 3, superimposed with numeric threshold results (dB) of fundus-guided microperimetry (MP-1; Nidek Technologies, Inc.); normal thresholds measured 20 dB at all locations shown. Despite quantifiable cones at several locations, we were unable to unambiguously identify cones in a parafoveal annulus at approximately 1° eccentricity. Visual function was reduced with perimetry values lower than 20 dB in regions with increased cone spacing. Additionally, CME, a feature commonly seen in patients with RP, was observed with high resolution using AOSLO in an RP patient (RP 1; Fig. 6A) and was detected on standard OCT (Fig. 6B). Despite the presence of cystoid spaces, cones were readily visualized and

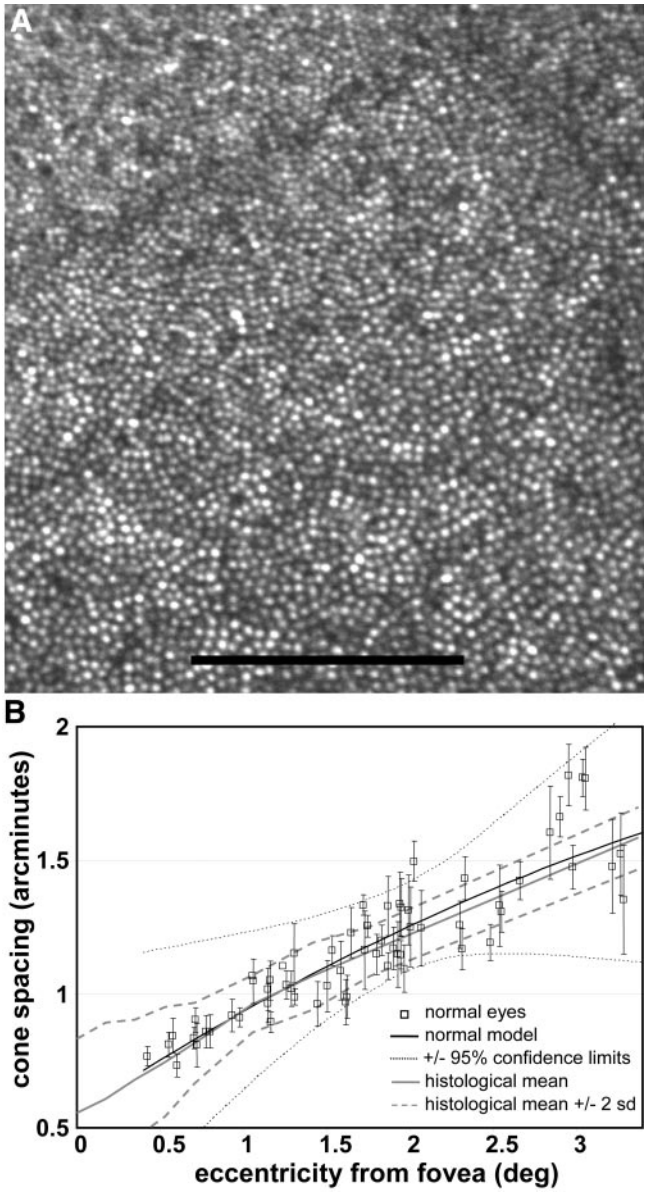

FIGURE 2. (**A**) Photoreceptor mosaic 1° from the fovea (*upper left*) from a healthy eye taken with AOSLO using a low-coherent 840-nm infrared source. Scale bar, 100 μm. (**B**) Quantitative measures of cone spacing for eight healthy eyes (*open squares*, mean ± 1 SD) were used to estimate normal mean cone spacing at different retinal eccentricities (*black solid line*) with 95% upper and lower PRs (*black dotted lines*) using a quadratic model. Normal predictive values are comparable to data from the literature obtained histologically (*gray solid line*, mean cone spacing measured from eight healthy eyes; *gray dashed lines*, mean ± 2 SD from mean cone spacing measured histologically[38]).

demonstrated normal cone spacing throughout the region, evaluated within 2° of fixation in RP 1.

Cone Spacing Abnormalities Correlated with Central Measures of Visual Function

Recognizing that all standard clinical measures of central macular function are of lower resolution than the single-cell resolution possible with AOSLO, we asked whether AOSLO cone spacing measured at a given location could be correlated with common central measures of visual function. Cone spacing at a single location, 1° eccentric to the fovea, was estimated from the curve for every patient and for three healthy eyes (subject ages 20, 27, and 61 years). Cone spacing measures were correlated with measures of central visual function, as shown in Figure 7. We observed significant correlations among several

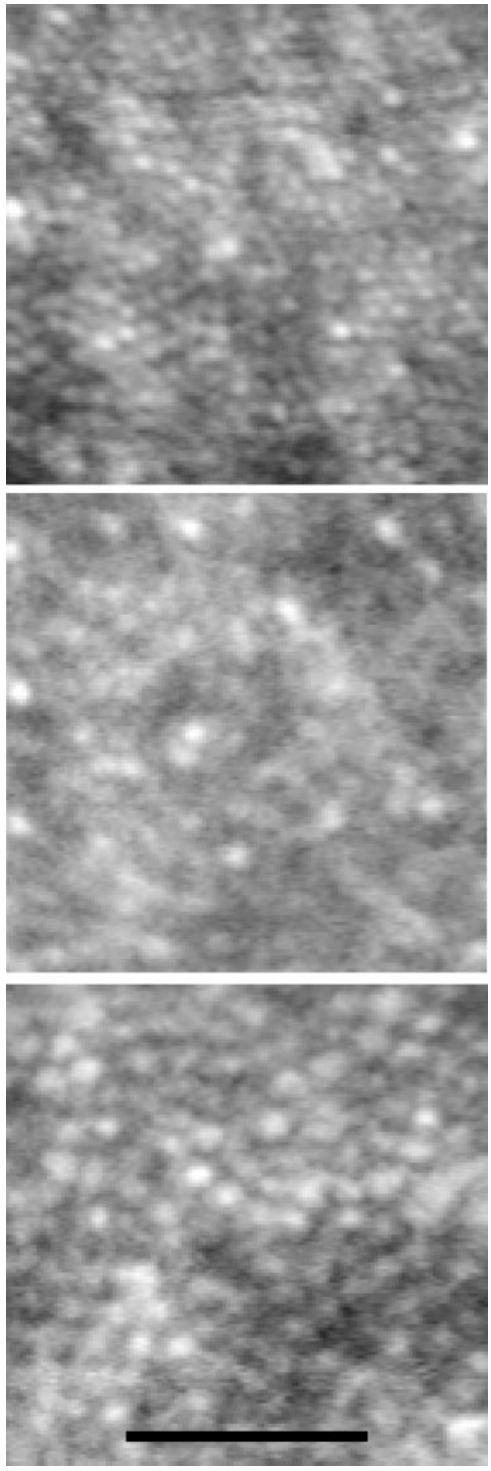

FIGURE 3. AOSLO cone montages taken from locations approximately 0.5° (approximately 150 μm) from the foveal center for a patient with simplex RP (RP 1; *top*), ADRP (RP 3; *middle*), and XL CRD (CRD 1; *bottom*). The cone mosaic of RP 1 is contiguous with normal cone spacing, whereas patchy regions of cone loss are seen adjacent to regions with more normal cone spacing in RP 3 with a rhodopsin mutation. The cone mosaic of CRD 1 is contiguous with increased cone spacing. Scale bar, 10 min arc or approximately 50 μm.

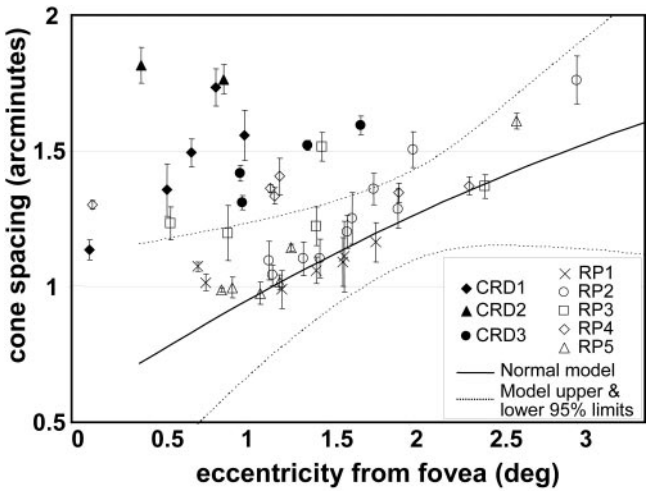

FIGURE 4. Quantitative AOSLO cone spacing in arcminutes from patients with RP (*open symbols*) and CRD (*filled symbols*). *Solid line*: mean estimated cone spacing for subjects with healthy eyes. *Dotted lines*: upper and lower 95% PR.

measures of macular cone function and cone spacing. Foveal threshold (Pearson $r = -0.88$, $P = 0.0003$), BCVA ($r = -0.73$, $P = 0.01$), and amplitude of the mfERG trace recorded within 1° of fixation ($r = -0.75$, $P = 0.008$) were negatively correlated with cone spacing (Figs. 7A–C). However, no significant correlation was identified between cone spacing and latency of the central multifocal ERG trace ($r = 0.50$, $P = 0.11$; Fig. 7D) or measures of central retinal thickness using OCT ($r = -0.59$, $P = 0.07$).

Intervisit Variability and Longitudinal Measures of Cone Spacing over Time

We studied the reproducibility of cone spacing measurements for two patients, one with RP (RP 1) and the other with XL CRD (CRD 1). Images were obtained on two occasions, separated by no more than 8 days. Figure 8 shows images of CRD 1 taken 3 days apart. Although the brightness of individual cones varies, as expected, in the two images,[12] identifiable landmarks are present in each image. For example, a region with bright profiles surrounded by darker ones is seen in each image (white boxes). Quantitative measures of cone spacing were made at three locations eccentric to fixation in which unambiguous cones could be identified at each session. Although these two patients did not provide enough data to make a statistical statement about variation between visits, agreement was good, with little or no change between imaging sessions. In each patient, the values differed by less than 0.01 arcminutes of cone spacing at each location, providing some evidence for similarity of cone spacing measurements across short time periods.

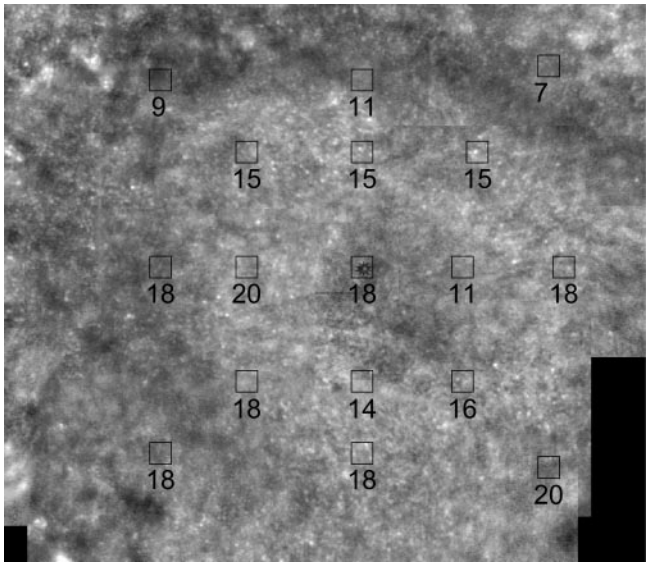

FIGURE 5. AOSLO images with fundus–guided microperimetry (MP-1; Nidek Technologies, Inc.) results superimposed within 2° of the preferred retinal locus of patient RP 3. Visual function is reduced in regions with increased cone spacing. Numeric values = patient thresholds; normal threshold values at all regions tested = 20 dB.

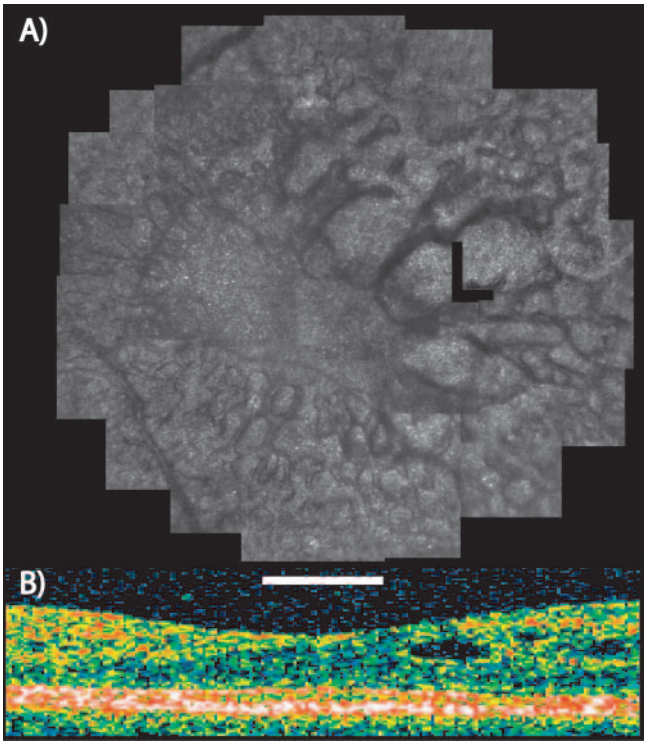

FIGURE 6. (**A**) AOSLO images of patient RP 1 show cyst walls of CME with high resolution. Cone spacing falls within 95% predictive values for subject with healthy eyes. Scale bar, 1° (approximately 300 μm). (**B**) OCT scan indicates CME.

DISCUSSION

We used AOSLO to evaluate macular cones in subjects with healthy eyes and in patients with two types of inherited retinal degenerative disease, RP and CRD. In contrast to earlier studies that used adaptive optics,[20,21] the infrared light source used in the present work provided higher-resolution images with improved fidelity by reducing interference artifacts and minimizing exposure to visible light during imaging. By examining a larger number of patients, we confirmed previous observations of increased cone spacing in affected persons and performed curve-fitting to estimate mean cone spacing with 95% PRs at different eccentricities for groups of patients with RP and CRD. We also identified genetic mutations in two patients and correlated high-resolution macular cone images with high-resolution fundus–guided perimetry and investigated short-term reproducibility of AOSLO cone measures.

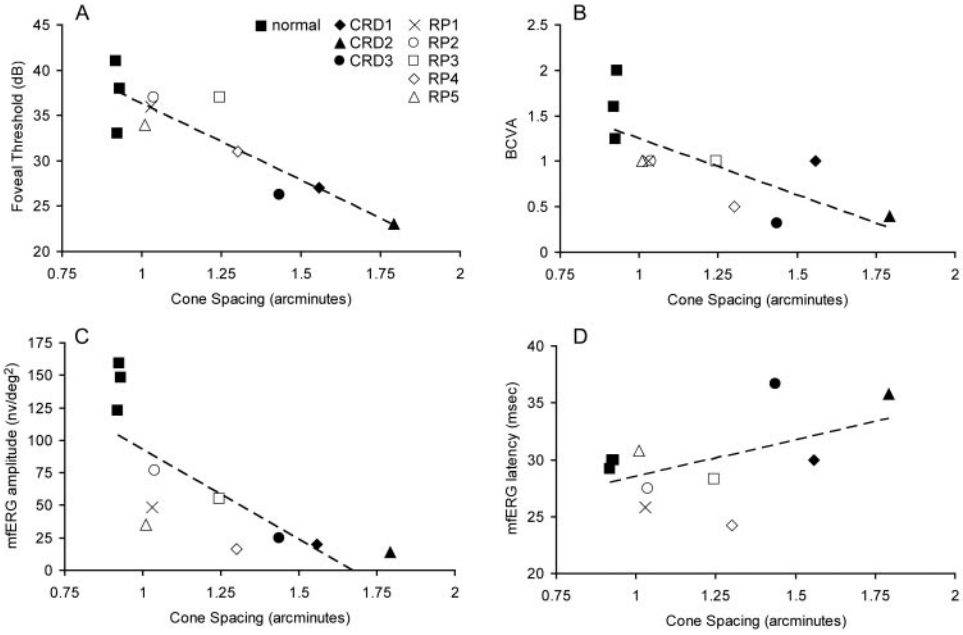

FIGURE 7. Foveal threshold (**A**), best-corrected visual acuity (**B**), and amplitude of the central mfERG P1 response (**C**) are significantly correlated with cone spacing, whereas timing of the central mfERG response is not (**D**). *Symbols* (other than filled squares) represent patients in Table 1; *filled squares* represent subjects with healthy eyes.

As previously reported,[20,21] CRD patients have regions of contiguous cone mosaics but increased spacing. The reflective properties of remaining cones in CRD patients degraded with abnormal spacing. This can be expected because histologic studies of CRD patients with advanced disease demonstrate increased cone pedicle size[40–42] and shortened outer segments.[32,40,41] It is not surprising that morphologic changes in the cones would disrupt the conditions that make them such excellent waveguides.[11] Reporting the nature of the reduction in cone density is important because cone loss in retinal disease can manifest in different ways. For example, images obtained with flood-illuminated AO from patients with congenital red-green color blindness revealed no cone enlargement despite a one-third reduction in spatial density.[13] These observations may yield insight into the process by which cones die, with the added advantage that measurements can be followed longitudinally in living patients and correlated with measures of visual function. Furthermore, AOSLO may provide a sensitive means of detecting retinal degeneration early in the course of disease. In

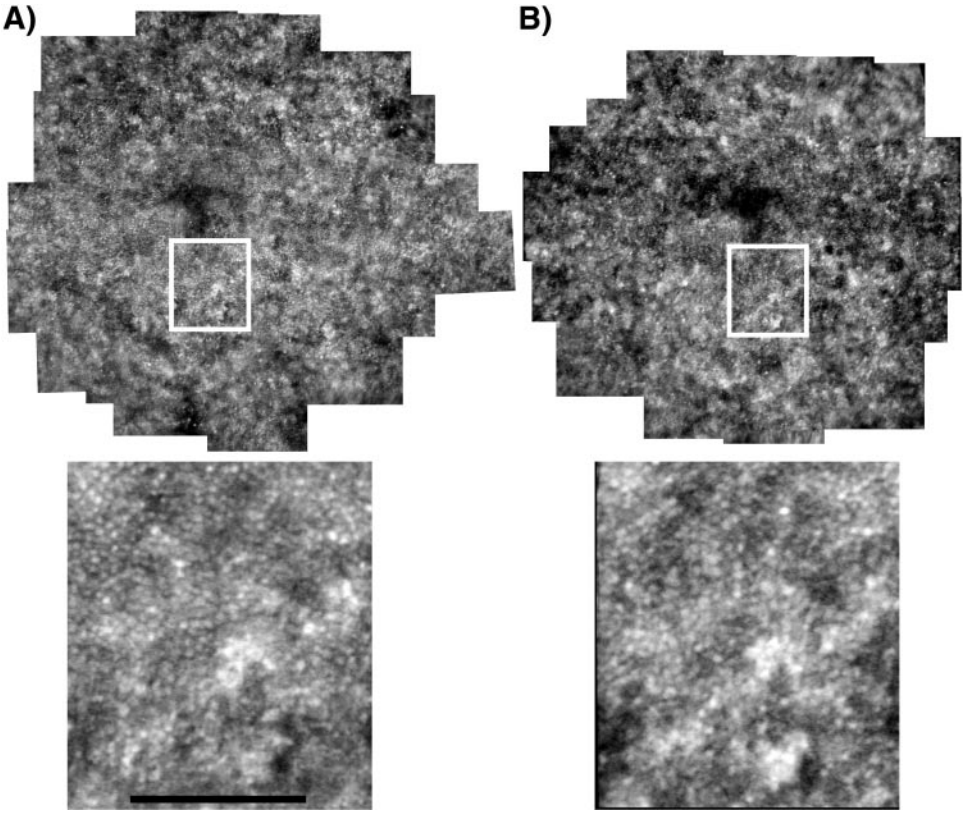

FIGURE 8. (**A**, **B**) AOSLO images taken on two separate sessions, 3 days apart, from a patient with XL CRD (CRD 1). Lower images are higher-magnification views of the *boxed* regions of the larger montage images. Individual cones can be distinguished in each image, though the brightness of each cone varies, as has been previously reported.[12]

addition, as therapies that prevent vision loss become available, earlier diagnosis may be of great value.

The genetic mutations underlying retinal degeneration were identified in two patients. A patient with ADRP (RP 3), carrying a rhodopsin mutation (Gly51Val), demonstrated a parafoveal annulus at approximately 1° eccentricity at which cones could not be unambiguously identified despite the presence of several other locations with quantifiable cones (Fig. 5). In regions with increased cone spacing, visual function was reduced, suggesting focal loss of cones resulting from this rhodopsin mutation. However, we could not rule out other mechanisms that might have contributed to reduced visual function in this patient. A patient with XL CRD (CRD 1) revealed a novel mutation near the 3′ end of the retinitis pigmentosa GTPase regulator (*RPGR*) gene in exon ORF15 (1443_1444 del GA). Although this patient's mutation has not been previously reported, other mutations in XL CRD patients have been identified in the 3′ region of ORF15.[29,32,33,43] Previously, a histologic study of a 69-year-old patient with a 1-nucleotide insertion in *RPGR*-ORF15 and clinical findings at age 40 similar to those of our patient demonstrated cone and rod loss with shortened outer segments in the macula and loss of regular cone spacing attributable to cell death.[32] The function of RPGR is not completely understood[44,45]; nevertheless, mice with altered RPGR function demonstrated progressive death of rods and cones, suggesting an essential role in the maintenance of photoreceptor function.[45,46] This study is the first to measure in vivo cone spacing in RP and CRD patients with known genetic mutations. Continued measurements may ultimately yield insight into the role rhodopsin and *RPGR* play in cone survival.

As in previous reports,[20,21] AOSLO cone spacing measures correlated significantly with foveal threshold, visual acuity, and mfERG amplitude in this study. By limiting our cone spacing measures to regions in which cones could be unambiguously identified, our estimates provided an extreme upper bound on the health of the mosaic. Choi et al.[20] had earlier correlated mfERG amplitude measures at different eccentricities with flood-illuminated AO images from three RP patients, one CRD patient, and one patient with juvenile macular dystrophy. Recognizing that mfERG responses often captured more than one region measured with AO, they chose to average cone densities, as determined by an automated averaging system, from the different represented regions. In contrast, we chose to correlate the central-most mfERG response amplitude with the cone spacing value estimated from a statistical model for each patient at a single location, 1° eccentric to the fovea, to avoid averaging the cone spacing measures from different eccentricities that might be represented by a single mfERG trace. Importantly, the findings of our study are similar to those of Choi et al.,[20] suggesting AO cone measures correlate well with measures of central visual function, even with different methods.

We found no significant correlation between cone spacing and central retinal thickness with OCT, probably because our measurements using standard clinical software did not provide the resolution necessary to measure photoreceptor outer segments quantitatively. However, more quantitative measures of OCT images[47–50] obtained by higher-resolution systems[51–53] may reveal a relationship. In addition, it is possible that subtle CME increased the retinal thickness measured from a single OCT scan. AOSLO images provide an extremely high-resolution, en face image of CME, a condition that affects many RP patients,[54,55] and the CME does not preclude imaging cones using AOSLO.

Finally, our data suggest that macular cones can be measured with excellent reproducibility over time in patients with RP and CRD. We observed cone spacing values that differed by no more than 0.01 arcminutes in repeated measures of two subjects, providing some evidence that AOSLO imaging can be performed reliably with little short-term variation.

In summary, we have used AOSLO to image macular cones with high resolution in subjects with healthy eyes and patients with retinal degenerative diseases. AOSLO provides a sensitive measure of cone structure in patients with retinal degeneration, both at early and advanced stages of the disease, and permits in vivo genotype–phenotype correlation of cone structure in patients with known genetic mutations. AOSLO cone parameters correlate well with measures of central visual function, which include visual acuity, foveal threshold, and mfERG amplitude. Cone spacing measures were reproducible in two patients, one with RP and another with CRD, suggesting that AOSLO imaging may be useful in monitoring cones during disease progression and in response to treatment.

Acknowledgments

The authors thank Barbara Grimes, PhD, and Charles E. McCulloch, PhD, for statistical assistance and consultation.

References

1. Cideciyan AV, Hood DC, Huang Y, et al. Disease sequence from mutant rhodopsin allele to rod and cone photoreceptor degeneration in man. *Proc Natl Acad Sci USA*. 1998;95:7103–7108.
2. Ripps H. Cell death in retinitis pigmentosa: gap junctions and the "bystander" effect. *Exp Eye Res*. 2002;74:327–336.
3. Leveillard T, Mohand-Said S, Fintz AC, Lambrou G, Sahel JA. The search for rod-dependent cone viability factors, secreted factors promoting cone viability. *Novartis Found Symp*. 2004;255:117–127; discussion 127–30, 177–178.
4. Leveillard T, Mohand-Said S, Lorentz O, et al. Identification and characterization of rod-derived cone viability factor. *Nat Genet*. 2004;36:755–759.
5. Liang J, Williams DR. Aberrations and retinal image quality of the normal human eye. *J Opt Soc Am A Opt Image Sci Vis*. 1997;14:2873–2883.
6. Liang J, Williams DR, Miller DT. Supernormal vision and high-resolution retinal imaging through adaptive optics. *J Opt Soc Am A Opt Image Sci Vis*. 1997;14:2884–2892.
7. Roorda A, Williams DR. The arrangement of the three cone classes in the living human eye. *Nature*. 1999;397:520–522.
8. Brainard DH, Roorda A, Yamauchi Y, et al. Functional consequences of the relative numbers of L and M cones. *J Opt Soc Am A Opt Image Sci Vis*. 2000;17:607–614.
9. Roorda A, Metha AB, Lennie P, Williams DR. Packing arrangement of the three cone classes in primate retina. *Vision Res*. 2001;41:1291–1306.
10. Neitz J, Carroll J, Yamauchi Y, Neitz M, Williams DR. Color perception is mediated by a plastic neural mechanism that is adjustable in adults. *Neuron*. 2002;35:783–792.
11. Roorda A, Williams DR. Optical fiber properties of individual human cones. *J Vision*. 2002;2:404–412.
12. Pallikaris A, Williams DR, Hofer H. The reflectance of single cones in the living human eye. *Invest Ophthalmol Vis Sci*. 2003;44:4580–4592.
13. Carroll J, Neitz M, Hofer H, Neitz J, Williams DR. Functional photoreceptor loss revealed with adaptive optics: an alternate cause of color blindness. *Proc Natl Acad Sci USA*. 2004;101:8461–8466.
14. Webb RH, Hughes GW, Delori FC. Confocal scanning laser ophthalmoscope. *Appl Optics*. 1987;26:1492–1499.
15. Dreher AW, Bille JF, Weinreb RN. Active optical depth resolution improvement of the laser tomographic scanner. *Applied Optics*. 1989;28:804–808.
16. Roorda A, Romero-Borja F, Donnelly WJ III, Queener H, Hebert TJ, Campbell MCW. Adaptive optics scanning laser ophthalmoscopy. *Opt Express*. 2002;10:405–412.

17. Romero-Borja F, Venkateswaran K, Roorda A, Hebert T. Optical slicing of human retinal tissue in vivo with the adaptive optics scanning laser ophthalmoscope. *Appl Opt*. 2005;44:4032–4040.
18. Zhang Y, Poonja S, Roorda A. MEMS-based adaptive optics scanning laser ophthalmoscopy. *Opt Lett*. 2006;31:1268–1270.
19. Zhang Y, Roorda A. Evaluating the lateral resolution of the adaptive optics scanning laser ophthalmoscope. *J Biomed Opt*. 2006;11: 014002.
20. Choi SS, Doble N, Hardy JL, et al. In vivo imaging of the photoreceptor mosaic in retinal dystrophies and correlations with visual function. *Invest Ophthalmol Vis Sci*. 2006;47:2080–2092.
21. Wolfing JI, Chung M, Carroll J, Roorda A, Williams DR. High-resolution retinal imaging of cone-rod dystrophy. *Ophthalmology*. 2006;113:1014–1019.e1.
22. Naash ML, Peachey NS, Li ZY, et al. Light-induced acceleration of photoreceptor degeneration in transgenic mice expressing mutant rhodopsin. *Invest Ophthalmol Vis Sci*. 1996;37:775–782.
23. Wang M, Lam TT, Tso MO, Naash MI. Expression of a mutant opsin gene increases the susceptibility of the retina to light damage. *Vis Neurosci*. 1997;14:55–62.
24. Organisciak DT, Darrow RM, Barsalou L, Kutty RK, Wiggert B. Susceptibility to retinal light damage in transgenic rats with rhodopsin mutations. *Invest Ophthalmol Vis Sci*. 2003;44:486–492.
25. Cideciyan AV, Jacobson SG, Aleman TS, et al. In vivo dynamics of retinal injury and repair in the rhodopsin mutant dog model of human retinitis pigmentosa. *Proc Natl Acad Sci USA*. 2005;102: 5233–5238.
26. Duncan T, Wiggert B, Whittaker N, Darrow R, Organisciak DT. Effect of visible light on normal and P23H-3 transgenic rat retinas: characterization of a novel retinoic acid derivative present in the P23H-3 retina. *Photochem Photobiol*. 2006;82:741–745.
27. Marmor MF, Holder GE, Seeliger MW, Yamamoto S. Standard for clinical electroretinography (2004 update). *Doc Ophthalmol*. 2004;108:107–114.
28. Marmor MF, Hood DC, Keating D, Kondo M, Seeliger MW, Miyake Y. Guidelines for basic multifocal electroretinography (mfERG). *Doc Ophthalmol*. 2003;106:105–115.
29. Demirci FY, Rigatti BW, Wen G, et al. X-linked cone-rod dystrophy (locus COD1): identification of mutations in RPGR exon ORF15. *Am J Hum Genet*. 2002;70:1049–153.
30. Yang Z, Peachey NS, Moshfeghi DM, et al. Mutations in the RPGR gene cause X-linked cone dystrophy. *Hum Mol Genet*. 2002;11: 605–611.
31. Rebello G, Vorster A, Greenberg J, et al. Analysis of RPGR in a South African family with X-linked retinitis pigmentosa: research and diagnostic implications. *Clin Genet*. 2003;64:137–141.
32. Demirci FY, Gupta N, Radak AL, et al. Histopathologic study of X-linked cone-rod dystrophy (CORDX1) caused by a mutation in the RPGR exon ORF15. *Am J Ophthalmol*. 2005;139:386–388.
33. Ebenezer ND, Michaelides M, Jenkins SA, et al. Identification of novel RPGR ORF15 mutations in X-linked progressive cone-rod dystrophy (XLCORD) families. *Invest Ophthalmol Vis Sci*. 2005; 46:1891–1898.
34. Stevenson SB, Roorda A. Correcting for miniature eye movements in high resolution scanning laser ophthalmoscopy. In: Manns F, Sodergerg P, Ho A, eds. *Ophthalmic Technologies XI*. Bellingham, WA: SPIE; 2005:145–151.
35. Vogel CR, Arathorn D, Roorda A, Parker A. Retinal motion estimation and image dewarping in adaptive optics scanning laser ophthalmoscopy. *Opt Express*. 2006;14:487–497.
36. Yellott JI Jr. Spectral analysis of spatial sampling by photoreceptors: topological disorder prevents aliasing. *Vision Res*. 1982;22:1205–1210.
37. Rodieck RW. The density recovery profile: a method for the analysis of points in the plane applicable to retinal studies. *Vis Neurosci*. 1991;6:95–111.
38. Curcio CA, Sloan KR, Kalina RE, Hendrickson AE. Human photoreceptor topography. *J Comp Neurol*. 1990;292:497–523.
39. Heckenlively JR, Weleber RG. X-linked recessive cone dystrophy with tapetal-like sheen: a newly recognized entity with Mizuo-Nakamura phenomenon. *Arch Ophthalmol*. 1986;104:1322–1328.
40. Rabb MF, Tso MO, Fishman GA. Cone-rod dystrophy: a clinical and histopathologic report. *Ophthalmology*. 1986;93:1443–1451.
41. Gregory-Evans K, Fariss RN, Possin DE, Gregory-Evans CY, Milam AH. Abnormal cone synapses in human cone-rod dystrophy. *Ophthalmology*. 1998;105:2306–2312.
42. Bonilha VL, Hollyfield JG, Grover S, Fishman GA. Abnormal distribution of red/green cone opsins in a patient with an autosomal dominant cone dystrophy. *Ophthalmic Genet*. 2005;26:69–76.
43. Mears AJ, Hiriyanna S, Vervoort R, et al. Remapping of the RP15 locus for X-linked cone-rod degeneration to Xp114–p211, and identification of a de novo insertion in the RPGR exon ORF15. *Am J Hum Genet*. 2000;67:1000–1003.
44. Khanna H, Hurd TW, Lillo C, et al. RPGR-ORF15, which is mutated in retinitis pigmentosa, associates with SMC1, SMC3, and microtubule transport proteins. *J Biol Chem*. 2005;280:33580–33587.
45. Shu X, Black GC, Rice JM, et al. RPGR mutation analysis and disease: an update. *Hum Mutat*. 2006;28:322–328.
46. Hong DH, Pawlyk BS, Shang J, Sandberg MA, Berson EL, Li T. A retinitis pigmentosa GTPase regulator (RPGR)-deficient mouse model for X-linked retinitis pigmentosa (RP3). *Proc Natl Acad Sci USA*. 2000;97:3649–3654.
47. Huang Y, Cideciyan AV, Papastergiou GI, et al. Relation of optical coherence tomography to microanatomy in normal and rd chickens. *Invest Ophthalmol Vis Sci*. 1998;39:2405–2416.
48. Huang Y, Cideciyan AV, Aleman TS, et al. Optical coherence tomography (OCT) abnormalities in rhodopsin mutant transgenic swine with retinal degeneration. *Exp Eye Res*. 2000;70:247–251.
49. Jacobson SG, Cideciyan AV, Iannaccone A, et al. Disease expression of RP1 mutations causing autosomal dominant retinitis pigmentosa. *Invest Ophthalmol Vis Sci*. 2000;41:1898–1908.
50. Schwartz SB, Aleman TS, Cideciyan AV, et al. Disease expression in Usher syndrome caused by VLGR1 gene mutation (USH2C) and comparison with USH2A phenotype. *Invest Ophthalmol Vis Sci*. 2005;46:734–743.
51. Ergun E, Hermann B, Wirtitsch M, et al. Assessment of central visual function in Stargardt's disease/fundus flavimaculatus with ultrahigh-resolution optical coherence tomography. *Invest Ophthalmol Vis Sci*. 2005;46:310–316.
52. Ko TH, Fujimoto JG, Schuman JS, et al. Comparison of ultrahigh- and standard-resolution optical coherence tomography for imaging macular pathology. *Ophthalmology*. 2005;112:1922.e1–1922.e15.
53. Wojtkowski M, Srinivasan V, Fujimoto JG, et al. Three-dimensional retinal imaging with high-speed ultrahigh-resolution optical coherence tomography. *Ophthalmology*. 2005;112:1724–1746.
54. Fishman GA, Fishman M, Maggiano J. Macular lesions associated with retinitis pigmentosa. *Arch Ophthalmol*. 1977;95:798–803.
55. Fishman GA, Maggiano JM, Fishman M. Foveal lesions seen in retinitis pigmentosa. *Arch Ophthalmol*. 1977;95:1993–1996.